Biogeosciences, 6, 439–451, 2009
www.biogeosciences.net/6/439/2009/
© Author(s) 2009. This work is distributed under
the Creative Commons Attribution 3.0 License.

Biogeosciences

Anthropogenic carbon distributions in the Atlantic Ocean: data-based estimates from the Arctic to the Antarctic

M. Vázquez-Rodríguez[1], F. Touratier[2], C. Lo Monaco[3], D. W. Waugh[4], X. A. Padin[1], R. G. J. Bellerby[5,6], C. Goyet[2], N. Metzl[3], A. F. Ríos[1], and F. F. Pérez[1]

[1]Instituto de Investigaciones Marinas, CSIC, Eduardo Cabello 6, 36208 Vigo, Spain
[2]IMAGES, Université de Perpignan, 52 avenue Paul Alduy, 66860 Perpignan, France
[3]LOCEAN/IPSL, Université Pierre et Marie Curie, case 100, 75252 Paris cedex 05, France
[4]Department of Earth and Planetary Sciences, Johns Hopkins University, Baltimore, USA
[5]Bjerknes Centre for Climate Research, University of Bergen, Allégaten 55, 5007 Bergen, Norway
[6]Geophysical Institute, University of Bergen, Allégaten 70, 5007 Bergen, Norway

Received: 4 March 2008 – Published in Biogeosciences Discuss.: 7 April 2008
Revised: 21 January 2009 – Accepted: 9 March 2009 – Published: 18 March 2009

Abstract. Five of the most recent observational methods to estimate anthropogenic CO_2 (C_{ant}) are applied to a high-quality dataset from five representative sections of the Atlantic Ocean extending from the Arctic to the Antarctic. Between latitudes 60° N–40° S all methods give similar spatial distributions and magnitude of C_{ant}. However, discrepancies are found in some regions, in particular in the Southern Ocean and Nordic Seas. The differences in the Southern Ocean have a significant impact on the anthropogenic carbon inventories. The calculated total inventories of C_{ant} for the Atlantic referred to 1994 vary from 48 to 67 Pg (10^{15} g) of carbon, with an average of 54±8 Pg C, which is higher than previous estimates. These results, both the detailed C_{ant} distributions and extrapolated inventories, will help to evaluate biogeochemical ocean models and coupled climate-carbon models.

1 Introduction

Understanding and modelling the marine carbon system is one of the pressing issues within the framework of climate change. Carbon dioxide, an important greenhouse gas, is being increasingly produced by human activities, adding to the "natural" carbon cycle. International research has made progressive efforts to monitor the evolution of the oceanic sink of atmospheric CO_2, and in understanding how human activities interfere with this air-sea coupled system. One of the grand aims of this effort is to accurately assess the future possible scenarios proposed by the Intergovernmental Panel on Climate Change (IPCC Fourth Assessment Report: Climate Change 2007[1]). The invasion of anthropogenic CO_2 (C_{ant}) in the ocean impacts not only the atmospheric carbon dioxide concentrations and is associated to climate change, but has also a direct effect on ocean chemistry, causing the so-called "ocean acidification" (Feely et al., 2004). The largest ocean acidification influences for the environment are expected to occur in the high northern and southern latitudes (Bellerby et al., 2005; Orr et al., 2005).

In this context, estimating C_{ant} concentrations in the oceans represents an important step towards a better evaluation of the global carbon budget and its rates of change. Since C_{ant} may not be directly measured in the ocean it has to be derived from in-situ observations, under several assumptions. The pioneering original works by Brewer (1978) and Chen and Millero (1979) addressed this issue, and estimated C_{ant} in Atlantic subsurface water masses of the Atlantic Ocean from total inorganic carbon (C_T) measurements. They corrected the measured C_T for the effect of organic matter remineralization (ROM) and made an estimate of the preformed Preindustrial C_T (C_T when the water was last in contact with the 1850 atmosphere). Together with the ROM contribution this preindustrial C_T was also subtracted from the observed C_T. In the last ten years, several observational (data-based) methods have been investigated at regional and global scales (see Wallace et al., 2001 for a historical overview). Two of

Correspondence to:
M. Vázquez-Rodríguez
(mvazquez@iim.csic.es)

[1]http://www.ipcc.ch/

them, the ΔC^* method (Gruber et al., 1996) and the Transient Time Distribution (TTD) method (Hall et al., 2002) have been applied at global scale. By using the ΔC^* approach, Sabine et al. (2004) estimated a global oceanic inventory of C_{ant} for a nominal year of 1994 of 118 ± 19 Pg C, which represents about 45% of the fossil fuel CO_2 emitted between 1800 and 1994. Similarly, Waugh et al. (2006) applied the TTD method to estimate the C_{ant} inventory for the global ocean and obtained results ranging between 94 and 121 Pg C for 1994. These authors also compared the C_{ant} distribution derived from the ΔC^* and TTD approaches and pointed out that in spite of the grand-scale reasonable agreement, substantial differences occurred in the North Atlantic, South-Eastern Atlantic and in all basins south of 30° S. This was an important result as it offered a range of C_{ant} concentrations to be used as a benchmark to be checked with ocean carbon cycle models. Analogous results were derived from intercomparison studies carried out with Ocean General Circulation Models (OGCM) (Orr et al., 2001), i.e.: reasonable agreement was found for ocean-wide inventories but significant differences prevailed at a regional scale in terms of inventory and as to where C_{ant} was actually located, especially in the high latitudes and between the upper and lower ocean. Estimating accurate oceanic C_{ant} inventories does not only provide a good constraint for predictive ocean models. They are also key input parameters in inverse models for calculating air-sea fluxes of C_{ant} (Gloor et al., 2003; Mikaloff-Fletcher et al., 2006; Gerber et al., 2009) and global budgets of the carbon cycle (IPCC, 2007).

In more recent years, additional data-based methods were developed in an attempt to improve the existing oceanic C_{ant} estimates, especially at a regional level. These are the TrOCA method (Touratier and Goyet, 2004; Touratier et al., 2007), the C°_{IPSL} method (Lo Monaco et al., 2005a) and the φC°_T method. To date, only few of these observational methods, including the ΔC^*, have been objectively inter-compared, and that is at regional scales only, namely: in the North Atlantic (Wanninkhof et al., 1999; Friis et al., 2006; Tanhua et al., 2007), the North Indian (Coatanoan et al., 2001), or along a single section in the Southern Ocean (Lo Monaco et al., 2005b). All of these studies identified significant discrepancies in C_{ant} distributions and specific inventories depending on the location, set of compared C_{ant} estimation approaches and methodological assumptions.

Today, there is a pressing need to compare and clarify the C_{ant} estimates from these various observational methods, as it has been analogously addressed in the case of ocean carbon models (OCMIP project; Orr et al., 2001), atmospheric inverse models (Gurney et al., 2004), or coupled climate-carbon models (C4MIP project[2]).

As a contribution to the European integrated project of CARBOOCEAN, this international collaborative study will focus on the comparison of results from five different approaches used to estimate anthropogenic CO_2 concentrations. This is done from a single and common high-quality data set from modern cruises conducted in the Atlantic Ocean, including the Arctic and Southern Ocean sectors. The results will identify the areas of greatest discrepancies and uncertainty amongst methods. Based on the fundamentals and main assumptions of the methods some adjustments will be proposed to try to improve the estimates and reconcile methods upon. In addition, the results will also serve observational and numerical ocean modellers to evaluate their simulations and will help to reach a consensus as to where C_{ant} is captured and actually stored. The analysis in the present work investigates the high latitudes (Southern Ocean and Nordic Seas) as locations where uncertainties are expected to be large for both data-based methods (Lo Monaco et al., 2005b; Waugh et al., 2006) and OGCMs (Orr et al., 2001). The Atlantic Ocean has been selected here because it has the largest C_{ant} specific inventory of all ocean basins, and also because of its large meridional and zonal gradients of C_{ant} (Sabine et al., 2004; Waugh et al., 2006). The paper first describes the various C_{ant} meridional and zonal distributions, according to the different methods applied, focusing on key areas (of water masses formation and transformation). The specific and total C_{ant} inventories are then presented and discussed on the basis of the main assumptions from the methods as possible sources for the observed dissimilarities.

2 Method

Data from four selected meridional sections (NSeas-Knorr, CLIVAR A16N, WOCE I06-Sb and WOCE A14) cover the length of the Atlantic and give a representative coverage of it (Fig. 1a). The WOCE AR01 extends from the Atlantic east to west ends at ∼24° N (Fig. 2a). They have all been recently conducted within the framework of either the WOCE or CLIVAR programs, except for the cruise in the Nordic Seas (NSeas, 2005) on board the R/V Knorr (Bellerby et al., 2005; Olsen et al., 2006). The data are available from the GLODAP website[3], except for the NSeas data[4] and the CLIVAR repeat section A16N legs 1 and 2 conducted during 2003[5]. The selected cruises correspond to different years and thus C_{ant} results had to be referred to the common year 1994 (GLODAP canonical year) to eliminate biases introduced by the effect of increasing fugacity of atmospheric CO_2 (fCO_2). This was done using data from time series of CO_2 molar fractions (xCO_2) and calculating from here the ratio of C_{ant} saturation concentrations for the year of the

[2] http://www.atmos.berkeley.edu/c4mip/

[3] http://cdiac.ornl.gov/oceans/glodap/Glodap_home.htm

[4] http://cdiac.ornl.gov/ftp/oceans/CARINA/Knorr/316N20020530/

[5] http://www.clivar.org/carbon_hydro/hydro_table.php

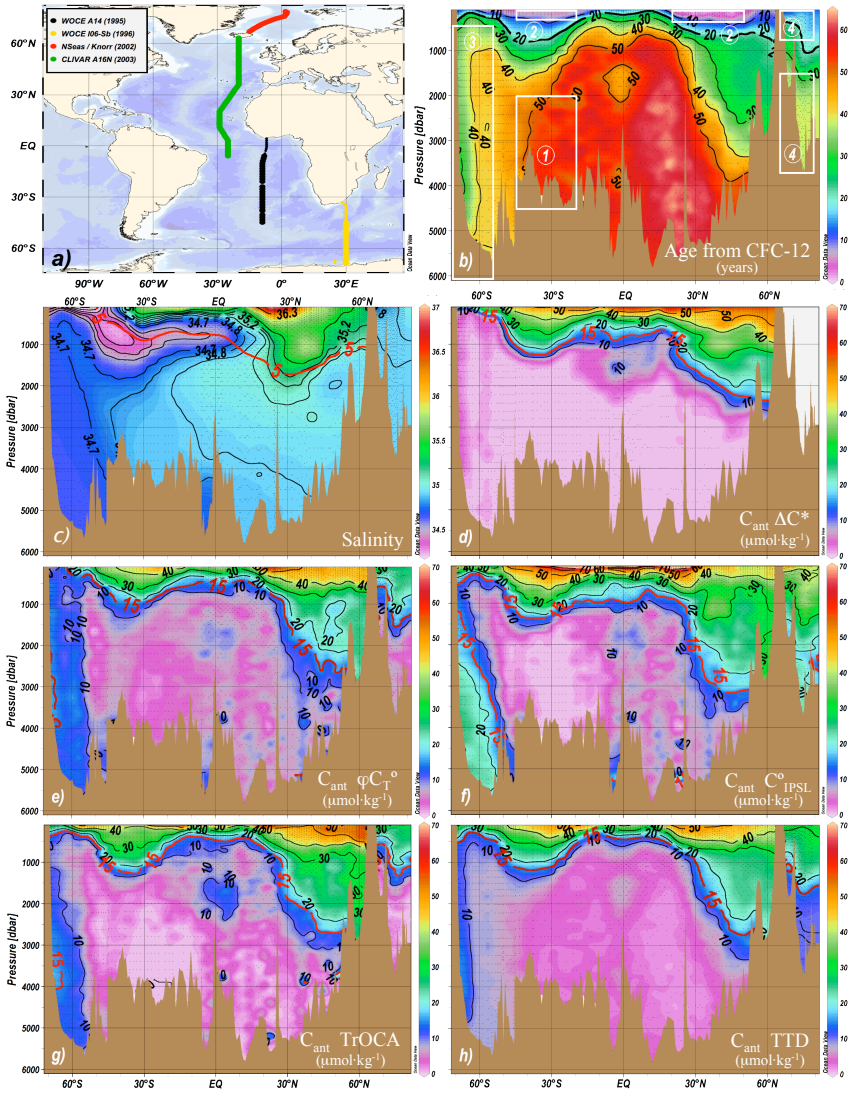

Fig. 1. (a) Map showing the considered meridional cruises WOCE A14, WOCE I06-Sb, CLIVAR A16N and NSeas/Knorr conducted in the Atlantic. Thinner dots in cruises A14 and I06-Sb represent stations not used (latitudinal overlapping of different cruises); **(b)** age (years) of water masses in the meridional transects from (a), calculated using CFC12. The inlayed rectangles delimit the regions where C_{ant} estimates are given a closer look, namely: 1=deep South Atlantic, 2=northern and southern subtropical gyres, 3=Southern Ocean and 4=The Nordic Seas; **(c)** salinity distribution of the meridional transect displaying the 5°C isotherm that separates the large volume of cold waters (~86% of the Atlantic Ocean volume) from warmer surface waters; (**d–h**) estimates of anthropogenic CO_2 (μmol kg^{-1}) in the meridional transect from the ΔC^*, φC_T°, C°_{IPSL}, TrOCA and TTD methods, respectively. The red 15 μmol kg^{-1} isopleth separates the region of maximum C_{ant} gradient from deeper waters.

cruise and the preindustrial era. The correction typically varied between 1–7 μmol kg^{-1} of C_{ant} depending on the sampling year, the potential temperature and salinity of the samples. Another consideration has been the overlapping latitudes of the A16N-A14 and A14-I06Sb section pairs. The general selection criteria followed was choosing the stations that were deepest and had the least influence of Indian Ocean waters. Accordingly, the northernmost ends of the A14 and I06Sb cruises are omitted from the plots (Fig. 1a). Finally, negative C_{ant} estimates that were within the specific range of uncertainty in each method were set to zero (ad hoc), while values more negative than that were taken as outliers and excluded from subsequent analysis.

Five data-based methods for C_{ant} estimation have been considered in this study: the TTD (Waugh et al., 2006), the TrOCA (Touratier et al., 2007), the C°_{IPSL} (Lo Monaco et al., 2005a) and the φC_T°. The ΔC^* method has been included in this comparison, but it has not been applied to the same data-set. The C_{ant} results here shown correspond to the same cruises though (except for the NSeas-Knorr one), taken

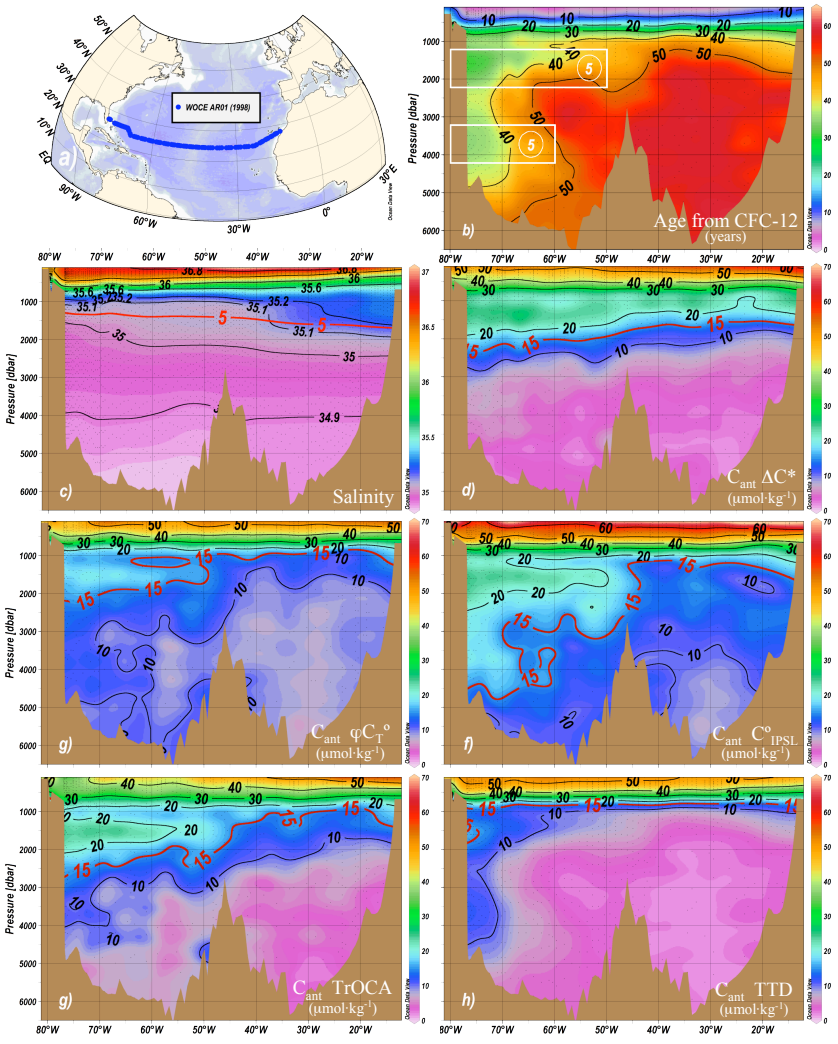

Fig. 2. Analogous contour plots to Fig. 1 for the zonal cruise WOCE AR01. From top to bottom and left to right: **(a)** cruise map, **(b)** CFC12 age in years showing the *u*DWBC and *l*DWBC limbs in white-contoured boxes numbered as "5"; **(c)** salinity field with the red 5°C isotherm overlaid; (**d–h**) C_{ant} concentration estimates (μmol kg^{-1}) from the ΔC*, φC_T°, C°_{IPSL}, TrOCA and TTD methods, respectively.

from the C_{ant} appearing in the GLODAP dataset as of Lee et al. (2003). They have applied the ΔC* method to evaluate the inventory of C_{ant} in the eastern and western basins of the Atlantic. Their C_{ant} estimates have been included in the global synthesis of Sabine et al. (2004) and the GLODAP database (Key et al., 2004). The data used and C_{ant} results obtained using the above methods are available under the Carboocean data portal to facilitate further comparisons with OGCM outputs, for instance, that are beyond the scope of the present work. The above methods can be classified into two groups on the basis of the variables needed to compute C_{ant}: a) the Transient-Tracer-based methods (TTD) that commonly use CFC11 or CFC12 concentration measurements as proxies of the anthropogenic CO_2 signal and b) the Carbon-based methods (ΔC*, C°_{IPSL}, φC_T° and TrOCA) which typically require measurements of dissolved inorganic carbon (C_T), total alkalinity (A_T), oxygen, temperature and eventually salinity and some nutrient analysis. They all make a steady-state assumption in terms of seasonal and interannual variability of the natural carbon cycle.

The Transient Time Distribution (TTD) is an indirect method that uses measurements of transient tracers (in particular CFCs) to estimate C_{ant} without the use of carbon measurements. The TTD method considers that there is a distribution of ventilation times (Hall et al., 2002), which is much more appropriate than the single ventilation time assumption from the early "shortcut" method by Thomas and Ittekot (2001). The considered transient time distribution assumes that advection (Γ) and mixing (Δ) processes are globally of the same order of magnitude (Δ/Γ=1). The air-sea

CO_2 disequilibrium is considered to be constant over time, but not in space. The use of pCFC12 age to calculate the date of formation of the water masses is a potential positive bias in the method. This is because the CFC12 history is shorter and more nonlinear than surface C_{ant}, and using the CFC12 age as the single ventilation means one looks too recently in the surface C_{ant} history and overestimates C_{ant} (Hall et al., 2002). This bias tends to increase with pCFC12 age, and is expected to be large for deep waters with pCFC12 ages greater than 25 years (Matear et al., 2003).

The classical ΔC^* approach is fundamentally based on the preformed C_T back-calculation principles established by Brewer (1978) and Chen and Millero (1979). To constitute a measure of C_{ant} in a water sample the method back-calculates the C_T of a water sample to its initial (preformed) C_T concentration when it was last at surface on the basis of the changes in A_T, AOU, salinity and θ. The ΔC^* approach is principally based on two assumptions: a) the anthropogenic CO_2 invasion has not altered surface alkalinity, so that it is unnecessary to differentiate between historical and present preformed alkalinity (A_T°) values and b) constant air-sea CO_2 disequilibrium (ΔC_{dis}) over time at the source region of the sampled water (steady state assumption). The method first introduced the ΔC_{dis} term to the back-calculation techniques and proposed a formal way to estimate it. In old water masses, according to a pCFC11 age criteria, C_{ant} was automatically set to zero and ΔC_{dis} was assigned the value of the quasi-conservative tracer ΔC^*. For younger water masses, the ΔC_{dis} had to be estimated using the "shortcut" method (Thomas and Ittekot, 2001) to calculate C_{ant} directly on those waters, based on their CFC11 content. One caveat to this procedure is that it can misleadingly prone to think that all waters void of CFCs are unaffected by C_{ant} (Matear et al., 2003). Knowingly, this conjecture introduces negative biases on the ΔC^* (Matsumoto and Gruber, 2005). It must alternatively be noticed that the ΔC^* approach considers that waters are fully saturated with oxygen and CFCs at the instant of their outcropping.

The C°_{IPSL} method is based on the original C° method described in the works by Brewer (1978) and Chen and Millero (1979). Differently, it allows for air-sea oxygen disequilibria. In most regions of the world ocean (including the North Atlantic) the preformed oxygen is close to equilibrium with the atmosphere. In the Southern Ocean, the upwelling of oxygen-exhausted waters provokes a deficit in surface oxygen concentrations of up to 50 μmol kg^{-1} (Poisson and Chen, 1987). A mean oxygen under-saturation coefficient α=12% calculated in the Weddell Sea area (Anderson et al., 1991) was used for C_{ant} calculation in ice-covered surface waters. This method uses different preformed relationships of A_T° and C_T° for southern and northern Atlantic waters. The relationships for the Southern Hemisphere were determined from winter data collected in surface waters (0–50 m) in the Atlantic and Indian Oceans. Northern relationships were determined using subsurface measurements (50–150 m) collected in the North Atlantic and Nordic Seas. The specific contributions of northern and southern waters are introduced in the equations via a specific north-south mixing ratio "k". The coefficients for each sample are determined with a multiple end-member mixing model they resolved via an optimum multiparameter (OMP) analysis. The R_C and R_N stoichiometric ratios used are the ones determined by Anderson and Sarmiento (1994). The preindustrial C_{ant} reference is calculated from North Atlantic Deep Water (NADW) detected in the South Atlantic, where C_{ant} concentrations are below detection limits. This zero-C_{ant} baseline reference corresponds to the increase in C_T° in the source region since the preindustrial era, and although it is a time-dependent parameter it is applied as a constant ($-51\,\mu$mol kg^{-1}).

The φC_T° method is another process-oriented biogeochemical approach to estimate C_{ant} in the Atlantic that follows the same fundamental principles as the ΔC^* or C°_{IPSL} back-calculation methods. The subsurface layer (100–200 m) is taken in the φC_T° method as a reference for characterising water mass properties at the moment of their formation. The air-sea disequilibrium (ΔC_{dis}) is parameterized at the subsurface layer first using a shortcut method to estimate C_{ant}. Since the average age of the water masses in the 100–200 m depth domain, and most importantly in outcropping regions, is under 25 years, the use of the shortcut method to estimate C_{ant} is appropriate (Matear et al., 2003). The A_T° and ΔC_{dis} parameterizations (in terms of conservative tracers) obtained from subsurface data are applied directly to calculate C_{ant} in the water column for waters above the 5°C isotherm and via an OMP analysis for waters with θ<5°C. This approach especially improves the estimates in cold deep waters that are subject to strong and complex mixing processes between Arctic and Antarctic water masses and represent an enormous volume of the global ocean (∼86%). One important aspect in this process is that none of the A_T° or ΔC_{dis} parameterizations are CFC-reliant. The φC_T° method proposes an approximation to the horizontal (spatial) and vertical (temporal) variability of ΔC_{dis} ($\Delta\Delta C_{dis}$) in the Atlantic Ocean in terms of C_{ant} and ΔC_{dis} itself. Also, the small increase of A_T° since the Industrial era due to $CaCO_3$ dissolution changes projected from models (Heinze, 2004) and the effect of rising sea surface temperatures on the parameterized A_T° are accounted for. These two last corrections are minor but should still be considered if a maximum 4 μmol kg^{-1} bias (2 μmol kg^{-1} on average) in C_{ant} estimates wants to be avoided.

The TrOCA method can be applied in the global ocean and it is based on a conservative tracer (the TrOCA) defined from oxygen, C_T and A_T, similarly to classical conservative tracers such as "NO" or "PO" (Broecker, 1974). It shares with other process-based C_{ant} methods its consideration of the $CaCO_3$ dissolution chemistry and the ROM processes as defined in the Redfilian equations. The C_{ant} concentration is estimated by subtracting from TrOCA a zero-C_{ant} reference (TrOCA°) defined from the "natural" concentrations of O_2, C_T and A_T. It is assumed that A_T is not affected by

Table 1. Summary statistics for the regions highlighted in Figs. 1b and 2b.

Region	Lat.	Long.	Depth (m)	θ (°C)	Salinity	pCFC12 (pmol/kg)	Age CFC12 (years)	AOU (μmol/kg)	C_{ant} ΔC^* (μmol/kg)	C_{ant} φC_T° (μmol/kg)	C_{ant} C°_{IPSL} (μmol/kg)	C_{ant} TrOCA (μmol/kg)	C_{ant} TTD (μmol/kg)
Deep South Atlantic	20° S–45° S	8° W	> 2000	2.0±0.3	34.85±0.04	0.01±0.01	53±4	100.7±11	0.1±0.5	3.3±0.2	0.2±0.5	0.4±1.0	2.8±0.1
N. Subtropical Gyre	20° N–50° N	20° W	100–350	15.6±2.6	36.18±0.43	1.56±0.19	4±4	31.3±21	42.8±0.6	48.7±0.5	50.1±0.9	47.8±0.5	46.1±0.4
S. Subtropical Gyre	20° S–45° S	8° W	100–300	13.1±3.5	35.19±0.46	1.40±0.21	7±2	29.2±18	44.0±0.6	41.3±0.7	52.3±1.0	37.8±0.6	43.8±0.4
Southern Ocean	55° S–72° S	30° E	> 500	0.1±0.6	34.68±0.02	0.19±0.13	37±4	125.6±11	1.5±1.6	12.8±0.1	16.4±0.4	11.1±0.2	9.9±0.1
upper Nordic Seas	65–79° N	0–20° W	100–750	−0.2±0.5	34.88±0.05	2.50±0.46	17±4	25.7±12	Null	23.2±1.1	38.2±1.1	24.2±1.2	28.1±0.5
lower Nordic Seas	65–79° N	0–20° W	> 1500	−1.0±0.1	34.91±0.01	0.50±0.03	36±3	56.0±5	Null	6.4±0.8	20.9±1.1	4.1±1.2	11.3±0.5
upper DWBC	24° N	50° W–80° W	1200–2200	4.1±0.6	35.02±0.04	0.25±0.17	38±7	61.2±10	21.9±0.5	16.5±0.4	22.1±0.4	21.0±0.5	10.9±0.4
lower DWBC	24° N	60° W–80° W	3200–4200	2.1±0.1	34.91±0.01	0.21±0.10	39±5	57.7±4	6.0±0.6	11.1±0.5	17.3±0.5	9.9±1.0	9.6±0.3

the increase of atmospheric CO_2 (Chen and Millero, 1979; Goyet et al., 1999), i.e. $A_T^\circ = A_T$; and that $O_2^\circ \approx O_2$. The equation for the reference term TrOCA° is a function of θ and A_T. This equation is derived from $\Delta^{14}C$ and corresponding to water parcels that can be assumed to be free of C_{ant}. When the concentration of $\Delta^{14}C < 175$ per mille, the approximate age of the corresponding water mass is greater than 1400 years, long before the beginning of human CO_2 massive emissions. The samples with maximum CFC11 concentrations, typically between 262.9 and 271.3 pptv corresponding to surface waters in 1992–1995 (maximum atmospheric pCFC11), were also selected as part of the dataset to obtain the TrOCA° expression.

3 Results and discussion

3.1 Anthropogenic CO_2 distributions

The meridional distributions of C_{ant} calculated from the ΔC^*, φC_T°, C°_{IPSL}, TrOCA and TTD methods are shown in Fig. 1d–h, respectively. The spatial patterns are similar in all calculations. The maximum C_{ant} values (40–60 μmol kg^{-1}) are consistently located in the northern subtropical gyre (20° N, 50° N), where the intensification of the Meridional Overturning Circulation (MOC) also provokes the strongest water mass outcrops and deepest C_{ant} transport. Alternatively, C_{ant} minima are unanimously located under the southern subtropical gyre below 1500 m, where the oldest water masses are found in the Atlantic eastern basin (Fig. 1b). There is also general agreement in the area of largest C_{ant} gradients, just above the 15 μmol kg^{-1} isopleth. The strong water mass formation processes in the North Atlantic subpolar gyre (Schmitz, 1996) have a large effect on the dynamics of C_{ant} oceanic uptake. They provoke the different C_{ant} distributions observed in the Nordic Seas, where the 15 μmol kg^{-1} isoline shallows abruptly.

The results for the WOCE AR01 cruise (Fig. 2) show a similar degree of agreement to the meridional section just described. There are three distinctive features to the AR01 section: a) the upper 1000 m are characterised by a strong vertical C_{ant} gradient, from 60 to 20 μmol kg^{-1}; b) the minimum values (0–15 μmol kg^{-1}) are consistently located in the eastern Atlantic Basin; c) the entrainment eastwards of the Deep Western Boundary Current (DWBC) upper limb is detected unanimously around 1500 m, whereas its lower limb (3000–4000 m) is not always as clearly seen in the C_{ant} fields.

In spite of the similarities in the large-scale C_{ant} distributions, there are some significant variations at a regional scale, most notably in the Antarctic Bottom Water (AABW) and the Nordic Seas. Below we discuss in more detail the distributions in several different regions, shown as boxes in Figs. 1b and 2b (see also Table 1). For each region, the average values of several quantities are listed in Table 1, and the average C_{ant} concentration is plotted against pCFC12 in Fig. 3. Whenever two or more results from different methods are compared within a region, a hypothesis contrast is applied with confidence level α=0.05, considering the number of data (N) and using the population means of the standard errors of the mean ($\sigma/\sqrt{N}$). Vertical profiles of average C_{ant} concentrations for the latitudes or longitudes covered by the above regions are also shown in Fig. 4 (note that several of these profiles include two of the boxed regions shown in Figs. 1b and 2b).

To examine the differences between the various C_{ant} estimates we calculate statistics between all pairs of methods. Specifically we calculate the Root Mean Square Difference (RMSD), Pearson's product-moment correlation coefficient (R) and the ratio of variances (γ). These three statistics are used to form Taylor diagrams (Taylor, 2001), which are often used to compare models with data. The RMSD can be interpreted as the magnitude of variability of one method compared to the other one in each pair, similarly to what the standard deviation represents around the mean of a given data distribution. These statistics for each region are shown graphically in Fig. 5. These plots show large variations in the statistical quantities, with cases where two estimates agree

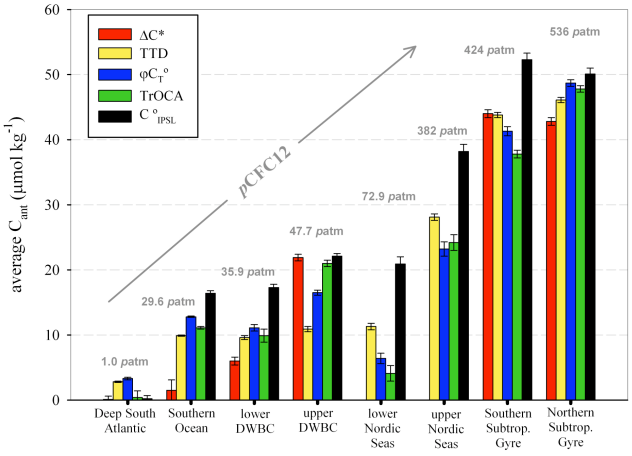

Fig. 3. Average regional C_{ant} estimates (μmol kg^{-1}) predicted by the five C_{ant} reconstruction methods here considered plotted in increasing order of average pCFC12 (patm) concentration on the studied regions. Notice that the pCFC12 scale is nominal and therefore non-linear. The error bars give the standard error of the mean ($\pm\sigma/\sqrt{N}$).

very well (i.e. low RMSD and R, and γ near unity) as well as other ones where there are large differences. These differences are discussed in more detail below, but in general, comparisons of the TTD estimates with the other estimates yield the largest differences, i.e., the highest RMSDs, lowest R, and values of γ furthest from unity. The φC°_{T} method generally shows the opposite: it generally has the lowest RMSDs, highest R, and γ values closest to unity. Interestingly, but perhaps not surprising, the carbon-based methods TrOCA, C°_{IPSL} and φC°_{T} come out highly correlated independently of the region considered.

3.1.1 Deep South Atlantic

The oldest water masses in the Atlantic are found in deep waters around 30° S and they are expected to have near-zero C_{ant} loads (Figs. 1b, 3 and Table 1). Deeper than 2000 m the average C_{ant} vertical profiles from all methods stabilize at very low values, however the actual values differ between methods, with ΔC^*, and C°_{IPSL} estimates being the lowest and TTD and φC°_{T} the largest (Fig. 4b). Most ΔC^* estimates for this region were either missing values or outliers and, therefore, excluded from inventory computations. In addition, the ΔC^* method defines its absolute zero-C_{ant} at the deep, very old waters based on CFC or $\Delta^{14}C$ age estimates. Analogous comments apply to the results from the C°_{IPSL} method, although this method does not report as many negative or missing values as in the ΔC^* case. The RMSD values in this region are low for all pairs of methods, which is likely related to the low average C_{ant} concentrations in the very old waters. The correlation between methods is general high, with the highest R for ΔC^*-φC°_{T} correlation (Fig. 5).

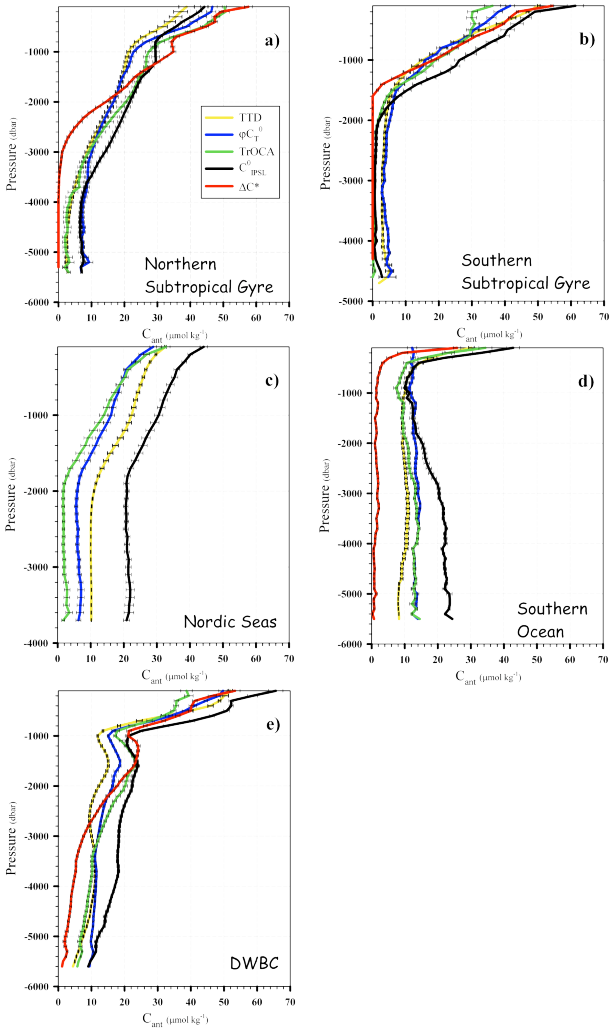

Fig. 4. Average vertical C_{ant} profiles (μmol kg^{-1}) of the selected regions in Figs. 1b and 2b. The C_{ant} estimates in each region were averaged over common depth intervals and the error bars represent the standard error of the mean ($\pm\sigma/\sqrt{N}$).

3.1.2 Subtropical gyres

The northern subtropical gyre, with an observed average age of 4 years (right-hand Box 2 in Fig. 1b), contains on average the highest C_{ant} concentrations and pCFC12 values (Fig. 3). The carbon-based methods TrOCA, C°_{IPSL} and φC°_{T} are all found to be significantly higher (p-level>0.995 in all cases) than the TTD estimate. The effect that the biology of the region could introduce via the R_C ratio is likely to have a minimum impact on results from the carbon-based methods, given the low apparent oxygen utilisation (AOU) average values. This makes the biological contribution an improbable source to this difference between TTD and carbon-based methods. Contradictorily, the average from the ΔC^* method, which is also carbon-based, is significantly lower than the

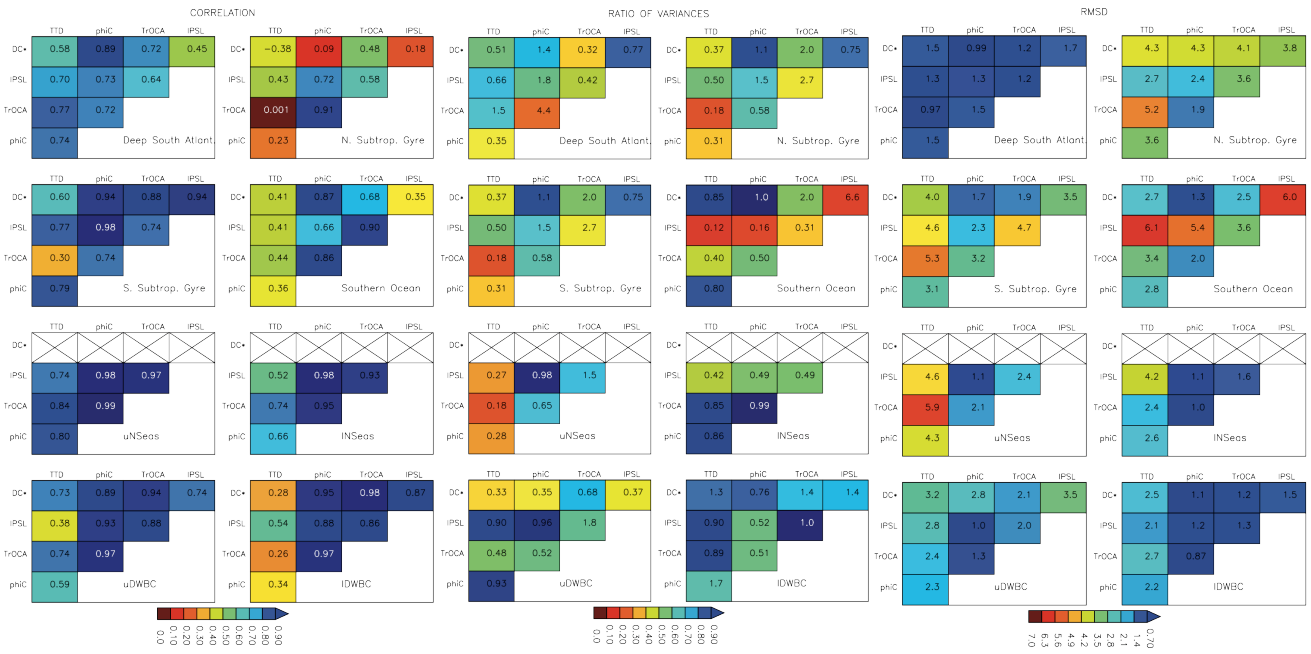

Fig. 5. Array of statistics for each of the regions highlighted in Figs. 1b and 2b. The Pearson's product-moment correlation coefficient (R), Root Mean Square Difference (RMSD, in μmol kg^{-1}) and ratio of variances (γ) were calculated for all method pairs. In all cases the more bluish the colour the better the agreement (dark blue for R=±1, RMSD=0, and γ=1). For the ratio of variances, γ and $1/\gamma$ are the same colour. Here, RMSD=$\sqrt{1/\mathrm{N}\sum_{i=1}^{\mathrm{N}}\left[\left(\mathrm{A}_i-\overline{\mathrm{A}}\right)-\left(\mathrm{B}_i-\overline{\mathrm{B}}\right)\right]^2}$, where A_i is the i-th C_{ant} estimate of the considered method "A" in the comparison pair, and "$\overline{\mathrm{A}}$" is the average of the subset of estimates considered from method "A". The terms B_i and "$\overline{\mathrm{B}}$" are analogously defined for method "B". N stands for the number of valid A-B data pairs.

TTD value by 3.3 μmol kg^{-1} (Fig. 3 and Table 1). The C_{ant} estimates in the southern subtropical gyre are similar to the northern counterpart, but with slightly lower average C_{ant} concentrations and less C_{ant} entrainment into the ocean interior (Fig. 4b and c). The above-described differences translate into different vertical C_{ant} gradients. In the southern subtropical gyre the C°_{IPSL} and ΔC^* have stronger vertical C_{ant} gradients than the rest of methods (Fig. 4b). This same pattern is observed in the northern subtropical gyre but it does not appear to be so clear due to the larger penetrations of C_{ant} in the water column (Fig. 4c). Lastly, it is worth noting from Figs. 1d–h and 4c that all methods detect the Mediterranean water (MW) influence, which causes a relative maximum of C_{ant} (average 22.6±3.5 μmol kg^{-1}) at about 1100 m depth at 37° N (Ríos et al., 2001; Álvarez et al., 2005; Aït-Ameur and Goyet, 2006). Large RMSDs are found for both subtropical gyres, and there is also a generalised tendency towards low correlation values. The most extreme values occur in the northern gyre, where there are generally very large RMSD and very low correlations between TTD and ΔC^* and the other methods, and between TTD and ΔC^*. In fact, out of all the studied regions and method pairs considered, the case of the TTD and ΔC^* in the northern subtropical gyre is the only where two methods have yielded C_{ant} estimates that are inversely correlated.

3.1.3 The Nordic Seas

Only four methods are compared in the Nordic Seas, as the GLODAP dataset (i.e., the ΔC^* method) did not include the 2005 NSeas-Knorr data used in this study. This region is characterised by moderate pCFC12 values (Fig. 3) and two well-defined layers in terms of C_{ant} with rather homogeneous concentrations (Figs. 1d–h and 4d). In the upper layer (100–750 m, upper Box 4 in Fig. 1b), the C°_{IPSL} approach gives the highest estimate (38.2±1.1 μmol kg^{-1}) followed by the TTD (28.1±0.5 μmol kg^{-1}), while the TrOCA and φC°_{T} methods give lower and similar values (24.2±1.4 and 23.2±1.1 μmol kg^{-1}, respectively). In the lower Nordic Seas (1500 m to bottom, lower Box 4 in Fig. 1b), all four methods produced different results and the discrepancies are larger than in the upper region (Figs. 3 and 4c): estimates from the TrOCA (4.1±1.2 μmol kg^{-1}) and the φC°_{T} (6.4±0.8 μmol×kg^{-1}) approaches are statistically lower, almost by half, than the TTD results. The C°_{IPSL} method gives the maximum C_{ant} estimate (20.9±1.1 μmol kg^{-1}), almost twice as large as the TTD method average value (11.3±0.5 μmol kg^{-1}), i.e., about the same trend of discrepancies observed in the deep Southern Ocean. The RMSDs cluster around a value of ∼1.5 μmol kg^{-1} except in the case of the TTD comparison pairs, where the RMSD is as large

as 5.9 μmol kg^{-1} (TTD-TrOCA). This gives an idea of how variable the average vertical C_{ant} profiles are with respect to the TTD, especially in the upper Nordic Seas. Nevertheless, the TTD vertical profile (Fig. 4c) represents quite the average of all methods in this region, most importantly in the lower Nordic Seas, and this is somewhat reflected by the associated R and γ values. The lowest γ for this region correspond to all method pairs involving the TTD ($\gamma\sim$0.22) and IPSL ($\gamma\sim$0.47) methods in the upper and lower Nordic Seas, respectively.

3.1.4 The Southern Ocean

South of 50° S the different methods, although applied to the same dataset, present very contrasting results. The average C_{ant} vertical profiles (Fig. 4d) share similar patterns: moderate values in the first 500 m before they suddenly drop into a plateau of almost constant concentrations in the rest of the water column. This trend is slightly different for C°_{IPSL} and φC°_{T}. For the former there is a tendency of C_{ant} to increase with depths below 1000 m, while the latter has a very stable vertical profile centred at $\sim$12.5 μmol kg^{-1}. The AABW forms in this region from Circumpolar Deep Water (CDW) and Ice Shelf Waters (ISW), potentially driving in the Southern Ocean an intense conveyance of C_{ant} down to the seafloor (>5000 m). The fact that C_{ant} may have penetrated this far down in the Southern Ocean is also suggested by the presence of CFC12 in the water column (Box 3 in Fig. 1b and Fig. 3). Consequently, the TTD method (based mainly on CFC12 data) produced C_{ant} down to the bottom at high latitudes, a signal that was not captured in the ΔC^* results (Figs. 3 and 4d) (Lo Monaco et al., 2005a, b; Waugh et al., 2006). Interestingly, the other methods (TrOCA, C°_{IPSL} and φC°_{T}) also detected significant C_{ant} concentrations in the deep and bottom waters of the Southern Ocean. The TTD, φC°_{T} and TrOCA methods have very similar vertical C_{ant} profiles below 1000 m (Fig. 4d). The ΔC^* predictions give close-to-zero C_{ant} values (1.5$\pm$1.6 μmol kg^{-1}) and are clearly lower than other estimates. The ΔC^* method assigns by default C_{ant}=0 references to old waters with low CFC concentrations, like those found below 500 m depths in the neighbouring regions of the South Atlantic (Gruber et al., 1996). Also, the ΔC^* approach assumes oxygen saturation in surface waters. The low results obtained in this area could follow from this assumption (Lo Monaco et al., 2005a). Nevertheless, it must be noted that authors like Sabine et al. (2002), by applying the ΔC^* method in other sectors of the Southern Ocean, have obtained higher C_{ant} estimates. The fact that the Southern Ocean is a large volume of water means that small differences between methods will ultimately translate in significant inventory differences in this region (Lo Monaco et al., 2005b). In terms of statistics, the largest RMSD values of all regions are found in this region, and there are also low correlation coefficients and γ far from unity, indicating how disparate are the C_{ant} estimates in this region.

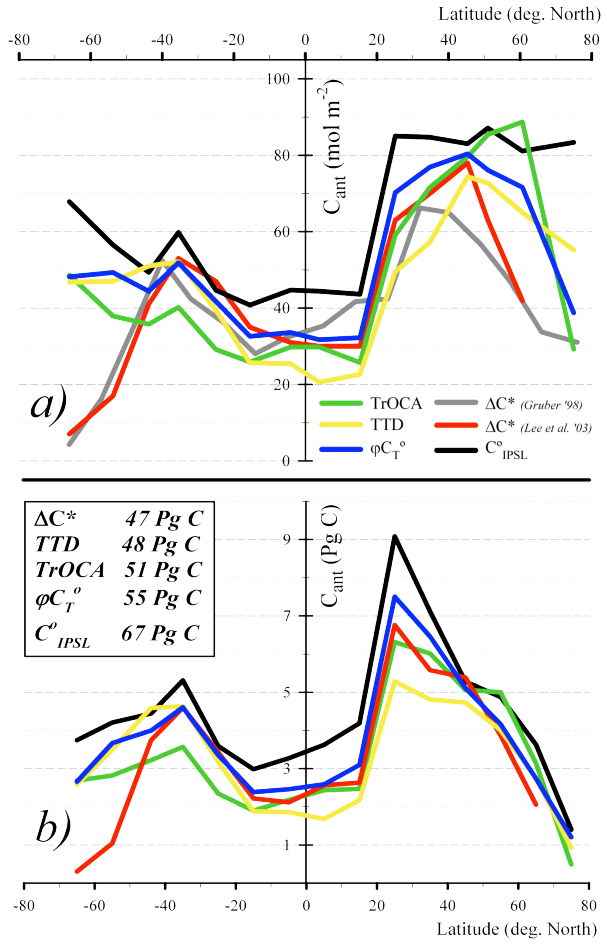

Fig. 6. Specific inventories **(a)** in mol m^{-2} for the whole Atlantic computed in latitude bands every 10°, after Lee et al., 2003. The total inventories (Pg C) for the same domain and latitude band resolution are plotted in **(b)**. The inlayed box gives the integrals of the presented total inventories (Pg C) for each method in the Atlantic Ocean.

3.1.5 The Deep Western Boundary Current (DWBC)

The DWBC is detected in C_{ant} from all methods (Fig. 2b). However, there are differences in the intensity of the vertical C_{ant} gradient generated by the upper limb (uDWBC), centred around 1500 m, and the lower limb (lDWBC), centred around 3500 m. The clearest signal in the DWBC is given by the C°_{IPSL} method, whilst the signal from the TTD approach is the weakest in terms of eastward penetration and vertical gradient between the two limbs (Figs. 3 and 4e). The TrOCA and ΔC^* methods display the largest gradient between limbs (Fig. 4e). However, when we compared the signal from the eastward lDWBC entrainment in both methods the TrOCA showed a well-defined limb, while the ΔC^* one was almost imperceptible. The φC°_{T} method gives values that are in the middle of the range from all methods (Table 1). Otherwise, it yields a weak lDWBC signal that is reproduced slightly

deeper than in the rest of methods. Finally, it is also notable that the eastward deflection and propagation of the North Atlantic Deep Water upper limb (uNADW) coming from the uDWBC (Weiss et al., 1985; Andrié et al., 1998) can also be observed in Fig. 1: a C_{ant} maximum located at 1500–2000 m depth in the Equator corresponding with a relative minimum of CFC12 age (∼50 yr) is detected to different extents by all methods. There are low RMSDs between most pairs of methods for both limbs. The methods are generally highly correlated and have similar variances. The TTD method is the exception with regard to the correlations, and there are low correlations between the TTD and other methods in the lDWBC.

3.2 Atlantic inventories of anthropogenic CO_2

To assess how the previous differences in the various data-based C_{ant} estimates affect the global C_{ant} budget, the results were integrated on the Atlantic basin scale. In calculating the inventory the following considerations were made: a) the water column integrals were calculated over the same 10-degree wide latitude bands as in Lee et al. (2003). In so doing, the results obtained can be compared with their estimates from the ΔC^* method; b) no in situ surface C_{ant} estimates were used at all so as to avoid the seasonal biogeochemical variability from surface layer data. Instead, values from the bottom limit of the winter mixed-layer were extended to 0 m, so that C_{ant} from surface waters is still being considered in inventory calculations (Lo Monaco et al., 2005b). On the basis of winter mixed layer depths the location of the bottom limits were placed at 100 m in subtropical and equatorial waters, and at 300 m for waters in the (33° S–50° S) latitude band; c) regarding total inventories, the meridional cruises used in this study belong to the eastern Atlantic basin. To tackle the zonal asymmetry assumption, results in Table 5 from Lee et al., 2003 were used. They provided specific inventories (mol m^{-2}) for the eastern and western basins and the total inventories (Pg C) for different latitude bands. A conversion factor per band of latitude (1.04±0.10) that accounted for the area was calculated using the eastern basin specific inventory and the total inventory data from Lee et al., 2003. Given the similarities here found in the general C_{ant} distributions it is assumed that the scaling obtained for the ΔC^* from Lee et al. (2003) can be applied to the rest of methods. Knowingly of the caveats attached to this practice, this assumption allows to calculate Atlantic inventories from the presented eastern Atlantic basin results; d) the C_{ant} inventories from Gruber (1998) and Lee et al. (2003) are included in Fig. 6a to show how the ΔC^* method yields very low values in the Southern Ocean, regardless of the dataset to which it is applied (Lo Monaco et al., 2005a). These inventories were calculated from different data collected over the same region here studied, and were referenced to year 1994; e) The errors for the specific inventories are of ±1 mol m^{-2} or ±2 mol m^{-2} when integrated down to 3000 m or 6000 m, respectively. They were calculated by means of random propagation of a 5 μmol kg^{-1} standard error of the Cant estimate with depth. Error bars in Fig. 6a are omitted for clarity.

All methods give reasonably similar specific inventories (Fig. 6a), except for the ΔC^* method in the Southern Ocean from either Gruber (1998) or Lee et al. (2003). The greatest similarities occur in the subtropical and equatorial regions, while some discrepancies between the C°_{IPSL}, φC°_T, TrOCA and TTD methods appear towards higher latitudes, especially north from 55° N, where none of the estimates converge. In the Southern Ocean (south of 55° S), the ΔC^* method shows extremely low values (10±5 mol m^{-2} on average) considering the non-negligible amount of CFCs found in this basin (Fig. 1b). These estimates are five to seven times lower than any other result in this area. The strong decreasing trend of the specific inventories according to the ΔC^* approach is also opposite to the other carbon-based methods which describe increasing specific inventories south from 45° S. More substantial differences were identified in other regions: in the Tropics, the TTD method gives about half the amount of C_{ant} the C°_{IPSL} method does, and in the North Atlantic differences of 20 mol m^{-2} are common.

The specific inventories were integrated by area to calculate the total inventories (in Pg C) over the same bands of latitude (Fig. 6b). In so doing, the aforementioned differences in the Nordic Seas diminish. All methods display an "M-shape" in the total inventory distribution, with a coherent maximum around 20–30° N and a relative maximum at 40–50° S. Although significant differences can still be seen between methods, we believe that the "M-shape" describes faithfully oceanic anthropogenic CO_2 fields and should be reproduced by ocean and climate models. The total inventories for the Atlantic basin (excluding the Nordic Seas), referred to 1994 estimated by the C°_{IPSL}, φC°_T, TrOCA and TTD methods are: 67, 55, 51 and 48 Pg C, respectively (average 55±8 Pg C; Fig. 6b). These results are higher than the 47 Pg C inventory given by Lee et al. (2003) using the ΔC^* approach, and if this ΔC^* estimate is to be included then the average C_{ant} inventory estimate for the Atlantic would drop to 54±8 Pg C. The main reason for the low inventory from the ΔC^* method comes mainly from the low C_{ant} concentrations predicted in the Southern Ocean (Fig. 1d), which alone represents 11–12% of the total inventory. The average C_{ant} inventories for the North and South Atlantic, considering all five methods, are 32±4 and 22±5 Pg C, respectively.

3.3 Discussion

The differences in the total inventories are mainly due to differences obtained for waters under the 5°C isotherm (Fig. 1c), which separates ∼86% of the Atlantic volume (excluding marginal seas) and divides the C_{ant} inventory by approximately half. This means that small errors in the estimation of C_{ant} have larger impacts in the inventories when they occur in θ<5°C waters. Some of the differences in these

waters can be linked to assumptions in the methods. For instance, the high estimates obtained with the C°_{IPSL} method in the Southern Hemisphere likely come from having overestimated the oxygen undersaturation in Antarctic surface waters, which would lead to C_{ant} overestimates (Lo Monaco et al., 2005a). For the TrOCA method low inventory estimates were identified in the South Atlantic (Fig. 6b). These are likely to derive from the large amount of close-to-zero C_{ant} estimates in the deep waters from the South Atlantic (Fig. 1g). The TTD method gives the lowest total inventory in the North Atlantic. This approach assumes the global constant Δ/Γ=1 and this constraint might not be representative of the North Atlantic (Steinfeldt et al., 2008). Here, the influence of the MOC makes advection gain importance over the mixing processes. Finally, the φC°_{T} method lacks extreme values at virtually any of the studied regions, although slightly low values are found in the upper 1000 m of the Nordic Seas. Also, it would be desirable that this method incorporated a more robust and complex OMP to resolve the water mass mixing in the Atlantic.

The assumptions made by the methodologies suggest that the causes for the disagreements may be due to: a) ice cap hindering of ventilation processes that alter the source properties of the water masses; b) the Alkalinity signal from the Arctic rivers is very different to the other waters of the world ocean; c) surface layer observations are normally used to parameterize properties, like preformed A_T (A°_{T}, i.e., A_T when the water mass outcrops) or air-sea CO_2 disequilibrium (ΔC_{dis}), that are later conveyed to the underlying isopycnals. The climate change driven shift of surface thermohaline characteristics would force the parameterizations to propagate wrong values towards the deeper ends of isopycnals, which have not sensed this thermal alteration yet. d) The North Atlantic Central Water (NACW) enters the surface North Atlantic and Norwegian Atlantic Current Systems with higher loads of anthropogenic CO_2 than they did in the past. This process causes the ΔC_{dis} driving C_{ant} uptake to diminish (Olsen et al., 2006). These factors introduce biases in the equations used to calculate C_{ant}.

In spite of the general convergence of the methods considered the choice of one data-based approach or another really depends on the region of interest, given the local variability of the results (Table 1, Fig. 6). Future revisions of the methods should focus on improving C_{ant} estimates in the Southern Ocean and Nordic Seas. These areas seem to be a determining issue in the discrepancies found for anthropogenic CO_2 burdens. The approximations of constant R_C ratios made by all carbon-based methods and the same relative weight given to advection and mixing (Δ/Γ=1, Waugh et al., 2006) at a global scale by the TTD method need to be relaxed. Finally, all methods involving water mass mixing calculations in their algorithms should strive to improve their own implementation of the intricate mixing issues in strong water mass formation regions, particularly in the northern Subpolar Gyre and Nordic Seas.

4 Conclusions

Five data-based methods (the TTD, ΔC^*, TrOCA, C°_{IPSL} and φC°_{T}) have been applied to a high-quality dataset to produce estimates of the C_{ant} distribution and inventory for the full length of the Atlantic Ocean. The differences between C_{ant} estimates are small in the Subtropics but larger for polar regions. The impact of these differences is most important in the Southern Ocean given its large contribution (up to 12%) to the total inventory of C_{ant}. The average C_{ant} Atlantic inventory of 54 ± 8 Pg C here obtained from the five methods suggests that previous estimates given by Gruber (1998) and Lee et al. (2003) could be underestimated. These differences in observational estimates should be considered in model-data comparisons. Furthermore, in addition to basin-scale comparisons, regional validation of models is encouraged as similar Atlantic inventories could result from diverse C_{ant} distributions.

It is worth noting that the large uncertainties in C_{ant} distributions identified in the Southern Ocean and Nordic Seas could lead to diverse scenarios and, henceforth, different conclusions regarding issues such as the carbon system saturation state and ocean acidification. Therefore, a multi data-based analysis combining outputs from observational and numerical models at different scales is strongly encouraged and should be addressed in the future. The results here shown will also help to better understand the evolution of the latitudinal atmospheric CO_2 gradient since the Preindustrial era, and how this is associated with the meridional transports of C_T on the long-time scale.

Acknowledgements. We would like to extend our gratitude to the Chief Scientists, scientists and crew who participated and put their effort in the oceanographic cruises utilized in this study, particularly to those responsible for the carbon, CFC, and nutrients measurements. The comments from two anonymous reviewers have been very valuable and constructive, and have greatly helped improving this work. This work was developed and funded by the European Commission within the 6th Framework Programme (EU FP6 CARBOOCEAN Integrated Project, Contract no. 511176). Marcos Vázquez-Rodríguez is funded by Consejo Superior de Investigaciones Científicas (CSIC) I3P predoctoral grant program REF. I3P-BPD2005.

Edited by: A. Bricaud

References

Aït-Ameur, N. and Goyet, C.: Distribution and transport of natural and anthropogenic CO_2 in the Gulf of Cadiz, Deep-Sea Res. II, 53, 1329–1343, 2006.

Álvarez, M., Pérez, F. F., Shoosmith, D. R., and Bryden, H. L.: The unaccounted role of Mediterranean Water in the drawdown of anthropogenic carbon, J. Geophys. Res., 110, 1–18. doi:10.1029/2004JC002633, 2005.

Anderson, L. G., Holby, O., Lindegren, R., and Ohlson, M.: The transport of anthropogenic carbon dioxide into the Weddell Sea, J. Geophys. Res., 96, 16679–16687, 1991.

Anderson, L. A. and Sarmiento, J. L.: Redfield ratios of remineralization determined by nutrient data analysis, Global Biogeochem. Cy., 8, 65–80, 1994.

Andrié, C., Ternon, J. F., Messias, M. J., Mémery, L., and Bourlès, B.: Chlorofluoromethanes distributions in the deep equatorial Atlantic during January–March 1993, Deep-Sea Res. I, 45, 903–930, 1998.

Bellerby, R. G. J., Olsen, A., Furevik, T., and Anderson, L. A.: Response of the surface ocean CO_2 system in the Nordic Seas and North Atlantic to climate change, in: Climate Variability in the Nordic Seas, edited by: Drange, H., Dokken, T. M., Furevik, T., Gerdes, R., and Berger, W., Geophysical Monograph Series, AGU, 189–198, 2005.

Brewer, P. G.: Direct observation of the oceanic CO_2 increase, Geophys. Res. Lett., 5, 997–1000, 1978.

Broecker, W. S.: "NO" a conservative water mass tracer, Earth Planet. Sci. Lett., 23, 8761–8776, 1974.

Chen, C.-T. A. and Millero, F. J.: Gradual increase of oceanic CO_2, Nature, 277, 205–206, 1979.

Coatanoan, C., Goyet, C., Sabine, C. L., and Warner, M.: Comparison of the two approaches to quantify anthropogenic CO_2 in the ocean: results from the northern Indian, Global Biogeochem. Cy., 15, 11–26, 2001.

Feely, R. A., Sabine, C. L., Lee, K., Berelson, W., Kleypas, J., Fabry, V. J., and Millero, F. J.: Impact of Anthropogenic CO_2 on the $CaCO_3$ System in the Oceans, Science, 305, 362–366, 2004.

Friis, K.: A review of marine anthropogenic CO_2 definitions: Introducing a thermodynamic approach based on observations, Tellus B, 58B, 2–15, doi:10.1111/j.1600-0889.2005.00173.x, 2006.

Gerber, M., Joos, F., Vázquez-Rodríguez, M., Touratier, F., and Goyet, C.: Regional air-sea fluxes of anthropogenic carbon inferred with an Ensemble Kalman Filter, Global Biogeochem. Cy., 23, GB1013, doi:10.1029/2008GB003247, 2009.

Gloor, M., Gruber, N., Sarmiento, J., Sabine, C. L., Feely, R. A., and Rödenbeck, C.: A first estimate of present and preindustrial air-sea CO_2 flux patterns based on ocean interior carbon measurements and models, Geophys. Res. Lett., 30(1), 1010, doi:10.1029/2002GL015594, 2003.

Goyet, C., Coatanoan, C., Eischeid, G., Amaoka, T., Okuda, K., Healy, R., and Tsunogai, S.: Spatial variation of total alkalinity in the northern Indian Ocean: a novel approach for the quantification of anthropogenic CO_2 in seawater, J. Mar. Res., 57, 135–163, 1999.

Gruber, N.: Anthropogenic CO_2 in the Atlantic Ocean, Global Biogeochemical Cycles, 12, 165-191, 1998.

Gruber, N., Sarmiento, J. L., and Stocker, T. F.: An improved method for detecting anthropogenic CO_2 in the oceans, Global Biogeochem. Cy., 10, 809–837, 1996.

Hall, T. M., Haine, T. W. N., and Waugh, D. W.: Inferring the concentration of anthropogenic carbon in the ocean from tracers, Global Biogeochem. Cy., 16(4), 1131, doi:10.1029/2001GB001835, 2002.

Heinze, C.: Simulating oceanic $CaCO_3$ export production in the greenhouse, Geophys. Res. Lett., 31, L16308, doi:10.1029/2004GL020613, 2004.

Key, R. M., Kozyr, A., Sabine, C. L., Lee, K., Wanninkhof, R., Bullister, J. L., Feely, R. A., Millero, F. J., Mordy, C., and Peng, T.-H.: A global ocean carbon climatology: Results from Global Data Analysis Project (GLODAP), Global Biogeochem. Cy., 18, GB4031, doi:10.1029/2004GB002247, 2004.

Kieke, D., Rhein, M., Stramma, L., Smethie, W. M., Bullister, J. L., and LeBel, D. A.: Changes in the pool of Labrador Sea Water in the subpolar North Atlantic, Geophys. Res. Lett., 34, L06605, doi:10.1029/2006GL028959, 2007.

Lee, K., Choi, S.-D., Park, G.-H., Wanninkhof, R., Peng, T.-H., Key, R. M., Sabine, C. L., Feely, R. A., Bullister, J. L., Millero, F. J., and Kozyr, A.: An updated anthropogenic CO_2 inventory in the Atlantic Ocean, Global Biogeochem. Cy., 17(4), 1116, doi:10.1029/2003GB002067, 2003.

Lo Monaco, C., Metzl, N., Poisson, A., Brunet, C., and Schauer, B.: Anthropogenic CO_2 in the Southern Ocean: Distribution and inventory at the Indian-Atlantic boundary (World Ocean Circulation Experiment line I6), J. Geophys. Res., 110, C06010, doi:10.1029/2004JC002643, 2005a.

Lo Monaco, C., Goyet, C., Metzl, N., Poisson, A., and Touratier, F.: Distribution and inventory of anthropogenic CO_2 in the Southern Ocean: Comparison of three data-based methods, J. Geophys. Res., 110, C09S02, doi:10.1029/2004JC002571, 2005b.

Matear, R. J., Wong, C. S., and Xie, L.: Can CFCs be used to determine anthropogenic CO_2, Global Biogeochem. Cy., 17(1), 1013, doi:10.1029/2001GB001415, 2003.

Matsumoto, K. and Gruber, N.: How accurate is the estimation of anthropogenic carbon in the ocean? An evaluation of the ΔC^* method, Global Biogeochem. Cy., 19, GB3014, doi:10.1029/2004GB002397, 2005.

Mikaloff-Fletcher, S. E., Gruber, N., Jacobson, A. R., Doney, S. C., Dutkiewicz, S., Gerber, M., Follows, M., Joos, F., Lindsay, K., Menemenlis, D., Mouchet, A., Müller, S. A., and Sarmiento, J. L.: Inverse estimates of anthropogenic CO_2 uptake, transport, and storage by the ocean, Global Biogeochem. Cy., 20, GB2002, doi:10.1029/2005GB002530, 2006.

Olsen, A., Omar, A. M., and Bellerby, R. G. J.: Magnitude and origin of the anthropogenic CO_2 increase and ^{13}C Suess effect in the Nordic seas since 1981, Global Biogeochem. Cy., 20, GB3027, doi:10.1029/2005GB002669, 2006.

Orr, J. E., Maier-Reimer, E., Mikolajewicz, U., Monfray, P., Sarmiento, J. L., Toggweiler, J. R., Taylor, N. K., Palmer, J., Gruber, N., Sabine, C. L., LeQuéré, C., Key, R. M., and Boutin, J.: Estimates of anthropogenic carbon uptake from four three-dimensional global ocean models, Global Biogeochem. Cy., 15(1), 43–60, 2001.

Orr, J. E., Fabry, V. J., Aumont, O., Bopp, L., Doney, S. C., Feely, R. A., et al.: Anthropogenic ocean acidification over the twenty-first century and its impact on calcifying organisms, Nature, 437 7059, 681–686, ISSN 0028-0836, doi:10.1038/nature04095, 2005.

Pérez, F. F., Vázquez-Rodríguez, M., Louarn, E., Padín, X. A., Mercier, H., and Ríos, A. F.: Temporal variability of the anthropogenic CO_2 storage in the Irminger Sea, Biogeosciences, 5, 1669–1679, 2008, http://www.biogeosciences.net/5/1669/2008/.

Poisson, A. and Chen, C. T. A.: Why is there little anthropogenic CO_2 in Antarctic Bottom Water, Deep Sea Res. A, 34, 1255–1275, 1987.

Ríos, A. F., Pérez, F. F., and Fraga, F.: Long term (1977–1997) measurements of carbon dioxide in the Eastern North Atlantic: evaluation of anthropogenic input, Deep-Sea Res. II, 48, 2227–2239, 2001.

Sabine, C. L., Feely, R. A., Gruber, N., Key, R. M., Lee, K., Bullister, J. L., Wanninkhof, R., Wong, C. S., Wallace, D. W. R., Tilbrook, B., Millero, F. J., Peng, T.-H., Kozyr, A., Ono, T., and Ríos, A. F.: The oceanic sink for anthropogenic CO_2, Science, 305, 367–371, 2004.

Schmitz Jr., W. J.: On the World Ocean Circulation: Volume I, Some Global Features/North Atlantic Circulation, Woods Hole Oceanographic Institution Technical Report WHOI-96-03, 1996.

Schuster, U. and Watson, A. J.: A variable and decreasing sink for atmospheric CO2 in the North Atlantic, J. Geophys. Res., 112, C11006, doi:10.1029/2006JC003941, 2007.

Sonnerup, R. E.: On the relations among CFC derived water mass ages, Geophys. Res. Lett., 28, 1739–1742, 2001.

Steinfeldt, R., Rhein, M., Bullister, J. L., and Tanhua, T.: Inventory changes in anthropogenic carbon from 1997–2003 in the Atlantic Ocean between 20° S and 65° N, Global Biogeochem. Cy., submitted, 2008.

Taylor, K. E.: Summarizing multiple aspects of model performance in single diagram, J. Geophys. Res., 106(D7), 7183–7192, 2001.

Thomas, H. and Ittekot, V.: Determination of anthropogenic CO_2 in the North Atlantic Ocean using water mass ages and CO_2 equilibrium chemistry, J. Mar. Sys., 27, 325–336, 2001.

Touratier, F. and Goyet, C.: Applying the new TrOCA approach to estimate the distribution of anthropogenic CO_2 in the Atlantic Ocean, J. Mar. Sys., 46, 181–197, 2004.

Touratier, F., Azouzi, L., and Goyet, C.: CFC11, Δ14C and 3H tracers as a means to assess anthropogenic CO_2 concentrations in the ocean, Tellus B, 59B, 318–325, doi:10.1111/j.1600-0889.2006.00247.x, 2007.

Vázquez-Rodríguez, M., Padin, X. A., Pérez , F. F., Ríos, A. F., and Bellerby, R. G. J.: Reconstructing preformed properties and air-sea CO_2 disequilibria for water masses in the Atlantic from subsurface data: An application in anthropogenic carbon determination, J. Mar. Sys., submitted, 2008.

Wallace, D. W. R.: Storage and transport of excess CO_2 in the oceans: the JGOFS/WOCE global CO_2 survey, in: Ocean Circulation and Climate, edited by: Siedler, G., Church, J., and Gould, J., Academic Press, San Diego, USA, 489–520, 2001.

Wanninkhof, R., Doney, S. C., Peng, T. H., Bullister, J. L., Lee, K., and Feely, R. A.: Comparison of methods to determine the anthropogenic CO_2 invasion into the Atlantic Ocean, Tellus B, 51B, 511–530, 1999.

Waugh, D. W., Hall, T. M., McNeil, B. I., Key, R., and Matear, R. J.: Anthropogenic CO_2 in the oceans estimated using transit time distributions, Tellus B, 58B, 376–389, doi:10.1111/j.1600-0889.2006.00222.x, 2006.

Weiss, R. F., Bullister, J. L., Gammon, R. H., and Warner, M. J.: Atmospheric chlorofluoromethanes in the deep equatorial Atlantic, Nature, 314, 608–610, 1985.